Early Detection and Rehabilitation Technologies for Dementia:

Neuroscience and Biomedical Applications

Jinglong Wu
Okayama University, Japan

Medical Information Science
REFERENCE

Senior Editorial Director:	Kristin Klinger
Director of Book Publications:	Julia Mosemann
Editorial Director:	Lindsay Johnston
Acquisitions Editor:	Erika Carter
Development Editor:	Myla Harty
Production Coordinator:	Jamie Snavely
Typesetters:	Mike Brehm, Jennifer Romanchak and Deanna Jo Zombro
Cover Design:	Nick Newcomer

Published in the United States of America by
Medical Information Science Reference (an imprint of IGI Global)
701 E. Chocolate Avenue
Hershey PA 17033
Tel: 717-533-8845
Fax: 717-533-8661
E-mail: cust@igi-global.com
Web site: http://www.igi-global.com/reference

Library of Congress Cataloging-in-Publication Data

Early detection and rehabilitation technologies for dementia: neuroscience and biomedical applications / Jinglong Wu, editor.
p. ; cm.
Includes bibliographical references and index.
Summary: "This book provides a comprehensive collection for experts in the Neuroscience and Biomedical technology fields, outlining various concepts from cognitive neuroscience and dementia to neural technology and rehabilitation"-- Provided by publisher.
ISBN 978-1-60960-559-9 (hardcover) -- ISBN 978-1-60960-560-5 (ebook) 1. Dementia--Diagnosis. 2. Neurologic examination. I. Wu, Jinglong, 1958-
[DNLM: 1. Dementia. 2. Brain--physiopathology. 3. Diagnostic Techniques, Neurological. 4. Early Diagnosis. WM 220]
RC521.E27 2011
616.8'3--dc22

2010054442

British Cataloguing in Publication Data
A Cataloguing in Publication record for this book is available from the British Library.

Chapter 28
Noninvasive Detection of Misfolded Proteins in the Brain Using [^{11}C]BF-227 PET

Nobuyuki Okamura
Department of Pharmacology, Tohoku University, Japan

Hiroyuki Arai
Institute of Development, Aging and Cancer, Tohoku University, Japan

Shozo Furumoto
Department of Pharmacology & Cyclotron and Radioisotope Center, Tohoku University, Japan

Yukitsuka Kudo
Innovation of New Biomedical Engineering Center, Tohoku University, Japan

Manabu Tashiro
Cyclotron and Radioisotope Center, Tohoku University, Japan

Kazuhiko Yanai
Department of Pharmacology, Tohoku University, Japan

Katsutoshi Furukawa
Institute of Development, Aging and Cancer, Tohoku University, Japan

ABSTRACT

Alzheimer's disease (AD) and many other neurodegenerative disorders belong to the family of protein misfolding diseases. These diseases are characterized by the deposition of insoluble protein aggregates containing an enriched β-sheet structure. To evaluate PET amyloid-imaging tracer [^{11}C]BF-227 as an agent for in vivo detection of various kinds of misfolded protein, a [^{11}C]BF-227 PET study was performed in patients with various protein misfolding diseases, including AD, frontotemporal dementia (FTD), dementia with Lewy bodies (DLB), sporadic Creutzfeldt-Jakob disease (sCJD) and Gerstmann-Sträussler-Scheinker disease (GSS). BF-227 binds to β-amyloid fibrils with high affinity. Most of the AD patients showed prominent retention of [^{11}C]BF-227 in the neocortex. In addition, neocortical retention of BF-227 was observed in the subjects with mild cognitive impairment who converted to AD during

DOI: 10.4018/978-1-60960-559-9.ch028

follow-up. DLB patients had elevated [^{11}C]BF-227 uptake in the neocortex. However, FTD and sCJD patients showed no cortical retention of [^{11}C]BF-227. Patients with multiple system atrophy had elevated BF-227 binding in the putamen. Finally, GSS patients had elevated BF-227 uptake in the cerebellum and other brain regions. This chapter confirms that BF-227 can selectively bind to α-synuclein and prion protein deposits using postmortem brain samples. Based on these findings, [^{11}C]BF-227 is not necessarily specific for β-amyloid in AD patients. However, this tracer could be used to detect various types of protein aggregates in the brain.

INTRODUCTION

Alzheimer's disease (AD) is the most common cause of dementia in the elderly. AD currently affects 4 million people in the United States and 15 million people globally. This disease begins insidiously with mild memory problems and progresses to the development of functional impairment in multiple cognitive domains within a few years. It is important to develop diagnostic methods that have adequate sensitivity and specificity to distinguish those who are likely to develop AD from those memory-impaired individuals who will not. The pathological hallmarks of AD are the deposition of senile plaques (SPs) and neurofibrillary tangles (NFTs) (Vickers et al., 2000). SPs and NFTs are mainly composed of β-amyloid (Aβ) protein and hyperphosphorylated tau protein, respectively. Aβ is a 4 kDa 39–43 amino acid metalloprotein product derived from the proteolytic cleavage of the amyloid precursor protein (APP) by β- and γ-secretases. The abnormal accumulation of SPs has been implicated as a central event in the etiology and the pathogenesis of AD and precedes the cognitive deterioration observed in AD (Okamura et al., 2008). Tau proteins accumulate in the neuronal cytoplasm and form NFTs with age. The initial lesions leading to NFTs occur in the transentorhinal cortex, followed by involvement of the entorhinal cortex and hippocampus, progressing to the neocortex. In vivo detection of SPs and NFTs in the brain enables the detection of AD patients in the pre-symptomatic stage. Noninvasive measurement of the amount of Aβ and tau deposits in the living brain is desirable for preventive interventions and assessment of therapeutic effects.

The density of SPs in brain tissue can be measured by molecular imaging techniques using positron emission tomography (PET) and a specific radiotracer. As Aβ deposits in the AD brain generally include the β-sheet fibrillar structure, many β-sheet binding agents have been developed as Aβ binding radiotracers for PET imaging. Currently, the most successful amyloid-binding agent is N-methyl-[^{11}C]2-(4'-methylaminophenyl)-6-hydroxybenzothiazol (PIB), which has been shown to possess a high affinity for Aβ fibrils. PIB-PET studies in human subjects have shown a robust difference between the retention pattern in AD patients and healthy controls, with AD cases showing significantly higher retention of PIB in the neocortical areas of the brain affected by Aβ deposition (Klunk et al., 2004). PIB retention in the neocortical areas is correlated with the Aβ plaque load (Ikonomovic et al., 2008). Benzoxazole derivatives are also promising alternatives for amyloid-imaging probes (Okamura et al., 2004; Furumoto et al., 2007). A PET study using ^{11}C-labeled 2-(2-[2-dimethylaminothiazol-5-yl]ethenyl)-6-(2-[fluoro]ethoxy) benzoxazole (BF-227) demonstrated retention of this tracer in the cerebral cortices of AD patients but not in those of normal subjects. AD patients were clearly distinguishable from normal individuals using neocortical uptake of [^{11}C]BF-227 (Kudo et al., 2007). Neocortical retention of BF-227 was observed in the subjects with mild cognitive impairment (MCI). BF-227 PET showed higher specificity and sensitivity than FDG-PET and

voxel-based morphometric analysis of MRI for differentiating between AD patients and normal controls, and between MCI converters and non-converters (Waragai et al., 2009; Furukawa et al., 2010). A voxel-by-voxel analysis demonstrated a higher retention of [^{11}C]BF-227, mainly in the posterior association cortex of AD patients and MCI converters. This distribution pattern corresponds well with the distribution of neuritic plaque deposits in postmortem AD brains. These findings suggest that [^{11}C]BF-227 is a promising PET probe for in vivo detection of dense amyloid deposits in AD patients.

AD and many other neurodegenerative disorders, including frontotemporal dementia (FTD), progressive supranuclear palsy, corticobasal degeneration, Parkinson's disease (PD), dementia with Lewy bodies (DLB), multiple system atrophy, and prion disease, belong to the family of protein misfolding diseases characterized by protein self-aggregation and deposition (Table 1). The tissue deposits observed in the brain in these diseases usually contain an enriched β-sheet structure, suggesting a potential target for non-invasive imaging using β-sheet binding agents. Thus, molecular PET imaging has the potential to be extended to this wide spectrum of protein misfolding diseases (Okamura et al., 2005; Okamura et al., 2009). The purpose of this study was to evaluate the clinical utility of [^{11}C]BF-227 PET for the noninvasive detection of misfolded proteins in the brain.

EXPERIMENT

Subjects

[^{11}C]BF-227 PET study was performed in 12 elderly normal controls, 14 patients with Alzheimer's disease (AD) and 12 subjects with mild cognitive impairment (MCI). The [^{11}C]BF-227 PET study was additionally performed in patients with frontotemporal dementia (FTD), dementia with Lewy bodies (DLB), multiple system atrophy (MSA), sporadic *Creutzfeldt-Jakob disease* (sCJD) and *Gerstmann-Sträussler-Scheinker* disease (GSS). The MCI subjects were divided into two groups: MCI converters (n=6) and MCI non-converters (n=7). The MCI converters were defined as patients who eventually developed AD within a mean follow-up of 27.0±7.9 months (range 14–30 months). The MCI non-converters were defined as having a transient memory loss or remaining cognitively stable through at least a two-year follow-up (27.7±2.2 months; range 25–30 months).

Table 1. Protein misfolding diseases and their fibrillar deposits

Protein	Fibrillar deposits	Diseases
Amyloid-β	Senile plaque Cerebrovascular amyloid	Alzheimer's disease Down syndrome Cerebral amyloid angiopathy
Tau	Neurofibrillary tangle Pick body Tufted astrocytes Astrocytic plaque	Alzheimer's disease Frontotemporal lobar degeneration Progressive supranuclear palsy Corticobasal degeneration
α-synuclein	Lewy body Glial cytoplasmic Inclusions	Parkinson's disease Dementia with Lewy bodies Multiple system atrophy
Prion	Prion plaque	Creutzfeldt-Jakob disease Gerstmann-Sträussler-Scheinker disease

Method

[^{11}C]BF-227 was synthesized from its precursor by N-methylation in dimethyl sulfoxide using [^{11}C]methyl triflate, as previously described (Kudo et al., 2007). The [^{11}C]BF-227 PET study was performed using a SET-2400W PET scanner (Shimadzu, Kyoto, Japan). After intravenous injection of 211–366 MBq [^{11}C]BF-227, dynamic PET images were obtained for 60 min (23 sequential scans; 5 scans × 30 s, 5 scans × 60 s, 5 scans × 150 s, and 8 scans × 300 s) with closed eyes. The standardized uptake value (SUV) was calculated by normalizing tissue concentrations by injected dose and body weight. Regions of interest (ROIs) were placed on co-registered axial MR images. The ROI information was then copied onto the PET images, and regional SUV values were sampled. The ratio of regional SUV to cerebellar SUV (SUVR) between 40 and 60 min post administration was calculated as an index of [^{11}C]BF-227 retention. For the analysis of prion disease data, we calculated regional to pons SUV ratio (SUVRp). For the analysis of MSA patient data, the distribution volume of [^{11}C]BF-227 was calculated by Logan's graphical analysis using arterial blood sample data. The protocol of this study was approved by the Committee on Clinical Investigation at Tohoku University School of Medicine and by the Advisory Committee on Radioactive Substances at Tohoku University. Written informed consent was obtained from all patients and control subjects after a complete description of the study. The clinical study was performed in accordance with the Declaration of Helsinki.

RESULTS

A PET study using [^{11}C]BF-227 demonstrated the retention of this tracer in the cerebral cortices of AD patients and MCI converters to AD but not in normal subjects or MCI non-converters (Figure 1). The average neocortical SUVR in BF-227 PET was significantly higher in the AD patients and MCI converters than in the normal subjects and MCI non-converters (Figure 2). We further examined BF-227 PET scans in patients with FTD, PD and DLB. Although imaging in FTD and PD patients showed normal distribution of BF-227 in the brain, DLB patients had moderate neocortical retention of BF-227 (Figure 1). Intriguingly, imaging from MSA patients showed BF-227 retention in the putamen, cerebral cortex and subcortical white matter. Microscopic examination indicates that BF-227 selectively binds to intracellular α-synuclein deposits, called glial cytoplasmic inclusions (GCIs), in MSA brain sections (Figure 3). Finally, significantly higher retention of BF-227 was detected in the cerebellum of GSS patients compared with that of normal controls and AD patients (Figure 4). In contrast, sCJD patients showed no obvious BF-227 retention in the cerebellum. Selective binding of BF-227 to prion protein plaques was confirmed using brain samples from autopsy-confirmed GSS cases (Figure 4).

DISCUSSION

Our study demonstrated that [^{11}C]BF-227 PET is useful for the in vivo detection of Aβ and prion protein plaques in the human brain. BF-227 PET achieved high diagnostic accuracy in discriminating between MCI converters and non-converters. This result strongly suggests that [^{11}C]BF-227 PET would be useful to predict conversion from MCI to AD. Regarding the binding of PET imaging agents to prion proteins, a previous PET study demonstrated a moderate level of FDDNP retention and no remarkable PIB retention in the brain of familial CJD patients (Boxer et al., 2007). Another PET study also demonstrated that PIB was not specifically retained in two sCJD patients (Villemagne et al., 2009). In comparison with these previous studies, BF-227 successfully

Figure 1. [^{11}C]BF-227 PET images in an elderly normal control, a patient with Alzheimer's disease (AD), a MCI non-converter, a MCI converter, a patient with frontotemporal dementia (FTD) and a patient with dementia with Lewy bodies (DLB).

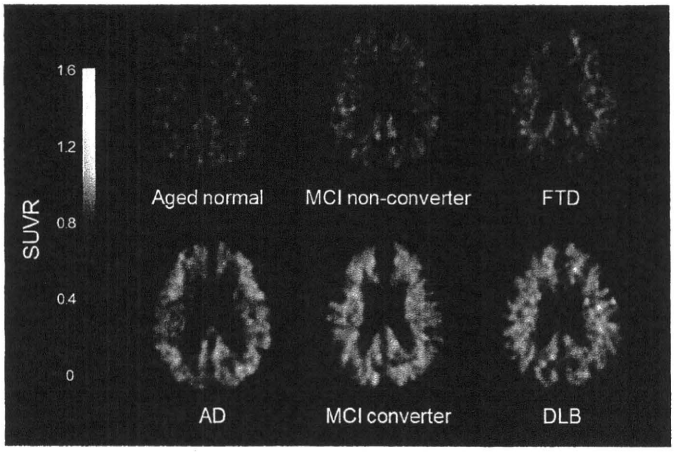

*Figure 2. Average neocortical SUVR values in elderly normal controls (AN), MCI non-converters (MCI-NC), MCI converters (MCI-C), and patients with Alzheimer's disease (AD). *p<0.05, ANOVA followed by a Bonferroni multiple comparisons test.*

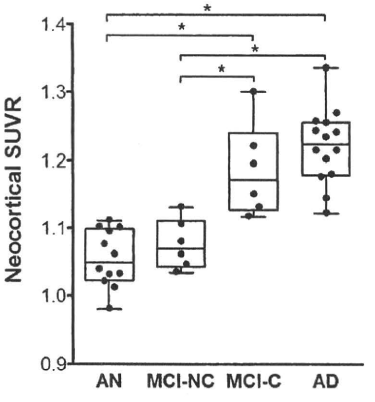

visualized prion protein plaques in the brains of GSS patients. Histopathological studies indicate a higher density of prion protein plaques in GSS patients than in familial CJD patients (Okamura et al., 2010). Therefore, the differences between our findings and those of previous studies would mainly depend upon the amount of prion protein fibrils in the brain. The difference might also be attributable to higher binding affinity of BF-227 to prion protein plaques compared to the other PET probes. Further analysis is necessary to compare the variable binding affinity of different PET probes for prion protein fibrils.

PET and microscopic studies also demonstrated that BF-227 has a potential ability to bind to and detect α-synuclein protein deposits in the brain. Previous PIB-PET studies have shown neocortical tracer accumulation in the brains of DLB patients. However, an in vitro binding study indicated that PIB failed to stain Lewy bodies in DLB brain sections. Considering the smaller size and lower density of Lewy bodies within the brains of DLB subjects relative to amyloid plaques, the contribution of Lewy bodies to the PET signals would be negligible. A recent study demonstrated that [^{18}F]BF-227 binds α-synuclein fibrils (Kd = 9.63 nM) with high affinity (Fodero-Tavoletti et al., 2009). Moreover, BF-227 labeled Lewy bodies and GCIs in fluorescence and immunohistochemical analyses of human brain sections, suggesting that BF-227 has higher binding affinity to α-synuclein deposits than PIB. Elevated BF-227 uptake was

Figure 3. (A): [^{11}C]BF-227 PET images in a normal control subject (Control) and a patient with multiple system atrophy (MSA). (B and C): Microscopic images of BF-227 staining (B) and α-synuclein immunostaining (C) of the cerebellar white matter of a MSA case. Bar = 100 μm.

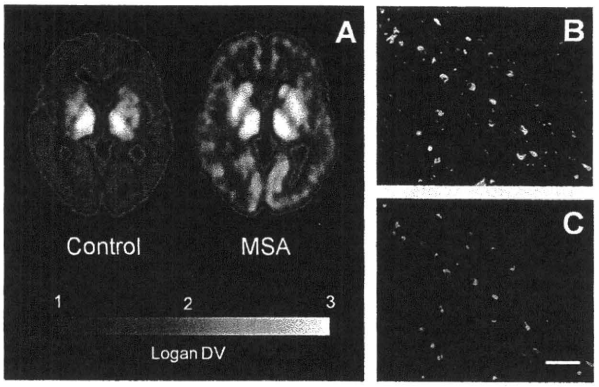

Figure 4. (A): The regional to pons SUV ratio (SUVRp) values in the cerebella of 10 normal controls, 17 patients with Alzheimer's disease (AD), 2 patients with sporadic Creutzfeldt-Jakob disease (sCJD), and 3 patients with Gerstmann-Sträussler-Scheinker disease (GSS). (B and C): Microscopic images of BF-227 staining (B) and PrP immunostaining (C) of the cerebellar cortex of a GSS case. Bar = 25 μm.

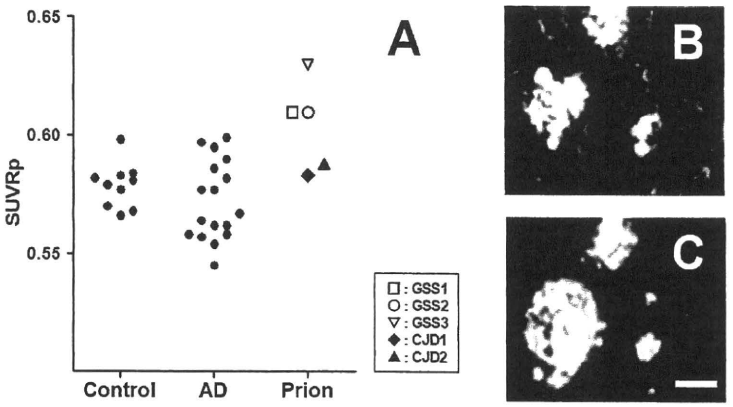

observed in the brains of MSA patients, which contain more α-synuclein deposits than those of DLB patients (Kikuchi et al., 2010). Further clinical studies of patients with α-synucleinopathy will clarify the potential of BF-227 for noninvasive detection of α-synuclein deposits in the human brain. From these findings, we conclude that BF-227 PET provides a potential method to facilitate both early diagnosis and noninvasive monitoring of protein misfolding diseases.

ACKNOWLEDGMENT

Part of this study was supported by the Health and Labor Sciences Research Grants for Translational Research from the Ministry of Health and the

Grant-in-Aid for Scientific Research on Priority Areas, Integrative Brain Research, from the Ministry of Education, Culture, Sports, Science, and Technology of Japan (20019006). We appreciate the technical assistance of Dr. R. Iwata, Dr. S. Watanuki, M. Miyake and Dr. Y. Ishikawa in the clinical PET studies, and Dr. K. Sugi and Dr. S. He in the imaging analysis. We also thank Dr. M. Higuchi for supporting the staining of human brain sections.

REFERENCES

Boxer, A. L., Rabinovici, G. D., Kepe, V., Goldman, J., Furst, A. J., & Huang, S. C. (2007). Amyloid imaging in distinguishing atypical prion disease from Alzheimer disease. *Neurology, 69*, 283–290. doi:10.1212/01.wnl.0000265815.38958.b6

Fodero-Tavoletti, M. T., Mulligan, R. S., Okamura, N., Furumoto, S., Rowe, C. C., & Kudo, Y. (2009). In vitro characterisation of BF227 binding to alpha-synuclein/Lewy bodies. *European Journal of Pharmacology, 617*, 54–58. doi:10.1016/j.ejphar.2009.06.042

Furukawa K., Okamura, N., Tashiro, M., Waragai, M., Furumoto, S., Iwata, R., ... Arai, H. (2010). Amyloid PET in mild cognitive impairment and Alzheimer's disease with BF-227: Comparison to FDG-PET. *Journal of Neurology*.

Furumoto, S., Okamura, N., Iwata, R., Yanai, K., Arai, H., & Kudo, Y. (2007). Recent advances in the development of amyloid imaging agents. *Current Topics in Medicinal Chemistry, 7*, 1773–1789. doi:10.2174/156802607782507402

Ikonomovic, M. D., Klunk, W. E., Abrahamson, E. E., Mathis, C. A., Price, J. C., & Tsopelas, N. D. (2008). Post-mortem correlates of in vivo PIB-PET amyloid imaging in a typical case of Alzheimer's disease. *Brain, 131*, 1630–1645. doi:10.1093/brain/awn016

Kikuchi, A., Takeda, A., Okamura, N., Tashiro, M., Hasegawa, T., Furumoto, S., ... Itoyama, Y. (2010). In vivo visualization of α-synuclein deposition by [^{11}C]-BF-227 PET in multiple system atrophy. *Brain*.

Klunk, W. E., Engler, H., Nordberg, A., Wang, Y., Blomqvist, G., & Holt, D. P. (2004). Imaging brain amyloid in Alzheimer's disease with Pittsburgh Compound-B. *Annals of Neurology, 55*, 306–319. doi:10.1002/ana.20009

Kudo, Y., Okamura, N., Furumoto, S., Tashiro, M., Furukawa, K., & Maruyama, M. (2007). 2-(2-[2-Dimethylaminothiazol-5-yl]ethenyl)-6-(2-[fluoro]ethoxy)benzoxazole: A novel PET agent for in vivo detection of dense amyloid plaques in Alzheimer's disease patients. *Journal of Nuclear Medicine, 48*, 553–561. doi:10.2967/jnumed.106.037556

Okamura, N., Fodero-Tavoletti, M. T., Kudo, Y., Rowe, C. C., Furumoto, S., & Arai, H. (2009). Advances in molecular imaging for the diagnosis of dementia. *Expert Opinion on Medical Diagnostics, 3*, 705–716. doi:10.1517/17530050903133790

Okamura, N., Furumoto, S., Arai, H., Iwata, R., Yanai, K., & Kudo, Y. (2008). Imaging amyloid pathology in the living brain. *Current Medical Imaging Reviews, 4*, 56–62. doi:10.2174/157340508783502840

Okamura, N., Shiga, Y., Furumoto, S., Tashiro, M., Tsuboi, Y., Furukawa, K., ... Doh-Ura, K. (2010). In vivo detection of prion amyloid plaques using [^{11}C]BF-227 PET. *European Journal of Nuclear Medicine and Molecular Imaging*.

Okamura, N., Suemoto, T., Furumoto, S., Suzuki, M., Shimadzu, H., & Akatsu, H. (2005). Quinoline and benzimidazole derivatives: Candidate probes for in vivo imaging of tau pathology in Alzheimer's disease. *The Journal of Neuroscience, 25*, 10857–10862. doi:10.1523/JNEUROSCI.1738-05.2005

Okamura, N., Suemoto, T., Shimadzu, H., Suzuki, M., Shiomitsu, T., & Akatsu, H. (2004). Styrylbenzoxazole derivatives for in vivo imaging of amyloid plaques in the brain. *The Journal of Neuroscience, 24*, 2535–2541. doi:10.1523/JNEUROSCI.4456-03.2004

Vickers, J. C., Dickson, T. C., Adlard, P. A., Saunders, H. L., King, C. E., & McCormack, G. (2000). The cause of neuronal degeneration in Alzheimer's disease. *Progress in Neurobiology, 60*, 139–165. doi:10.1016/S0301-0082(99)00023-4

Villemagne, V. L., McLean, C. A., Reardon, K., Boyd, A., Lewis, V., & Klug, G. (2009). ^{11}C-PiB PET studies in typical sporadic Creutzfeldt-Jakob disease. *Journal of Neurology, Neurosurgery, and Psychiatry, 80*, 998–1001. doi:10.1136/jnnp.2008.171496

Waragai, M., Okamura, N., Furukawa, K., Tashiro, M., Furumoto, S., & Funaki, Y. (2009). Comparison study of amyloid PET and voxel-based morphometry analysis in mild cognitive impairment and Alzheimer's disease. *Journal of the Neurological Sciences, 285*, 100–108. doi:10.1016/j.jns.2009.06.005

KEY TERMS AND DEFINITIONS

Alzheimer's Disease: The most common form of dementia.

Mild Cognitive Impairment (MCI): A diagnosis given to individuals who have cognitive impairments beyond that expected for their age and education but that do not interfere significantly with their daily activities.

Neurofibrillary Tangles: Pathological protein aggregates found within neurons in cases of Alzheimer's disease.

Positron Emission Tomography (PET): A nuclear medicine imaging technique that produces a three-dimensional image or picture of functional processes in the body.

Prion: An infectious agent that is primarily composed of protein.

Protein Misfolding Diseases: Clinically and pathologically diverse disorders in which specific proteins accumulate in cells or tissues of the body.

Senile Plaques: Extracellular deposits of amyloid in the gray matter of the brain.

Tau: A neuronal microtubule-associated protein found predominantly on axons.

α-Synuclein: The primary structural component of Lewy body fibrils.

β-Amyloid: A 39-43 amino acid peptide that appears to be the main constituent of senile plaques in the brains of Alzheimer's disease patients.

doi:10.1093/brain/awr038 Brain 2011: 134; 1089–1100 | 1089

BRAIN
A JOURNAL OF NEUROLOGY

^{18}F-THK523: a novel *in vivo* tau imaging ligand for Alzheimer's disease

Michelle T. Fodero-Tavoletti,[1,2] Nobuyuki Okamura,[3] Shozo Furumoto,[3] Rachel S. Mulligan,[4] Andrea R. Connor,[1,2] Catriona A. McLean,[5] Diana Cao,[6] Angela Rigopoulos,[6] Glenn A. Cartwright,[6] Graeme O'Keefe,[4] Sylvia Gong,[4] Paul A. Adlard,[1,7] Kevin J. Barnham,[1,2,7] Christopher C. Rowe,[4] Colin L. Masters,[7] Yukitsuka Kudo,[8] Roberto Cappai,[1,2] Kazuhiko Yanai[3] and Victor L. Villemagne[4,7]

1 Department of Pathology, The University of Melbourne, Victoria, 3010, Australia
2 Bio21 Molecular and Biotechnology Institute, The University of Melbourne, Victoria, 3010, Australia
3 Department of Pharmacology, Graduate School of Medicine, Tohoku University, Sendai, 980-8575, Japan
4 Department of Nuclear Medicine and Centre for PET, University of Melbourne, Austin Health, Victoria, 3084, Australia
5 Department of Anatomical Pathology, The Alfred Hospital, Victoria, 3181, Australia
6 Ludwig Institute for Cancer Research, Austin Hospital, Victoria, 3084, Australia
7 The Mental Health Research Institute, Victoria, 3010, Australia
8 Innovation of New Biomedical Engineering Centre, Tohoku University, Sendai, 980-8575, Japan

Correspondence to: Victor L. Villemagne,
Austin Health, Department of Nuclear Medicine and Centre for PET,
145 Studley Road,
Heidelberg,
VIC, 3084, Australia
E-mail: villemagne@petnm.unimelb.edu.au

While considerable effort has focused on developing positron emission tomography β-amyloid imaging radiotracers for the early diagnosis of Alzheimer's disease, no radiotracer is available for the non-invasive quantification of tau. In this study, we detail the characterization of ^{18}F-THK523 as a novel tau imaging radiotracer. *In vitro* binding studies demonstrated that ^{18}F-THK523 binds with higher affinity to a greater number of binding sites on recombinant tau (K18Δ280K) compared with β-amyloid$_{1-42}$ fibrils. Autoradiographic and histofluorescence analysis of human hippocampal serial sections with Alzheimer's disease exhibited positive THK523 binding that co-localized with immunoreactive tau pathology, but failed to highlight β-amyloid plaques. Micro-positron emission tomography analysis demonstrated significantly higher retention of ^{18}F-THK523 (48%; $P < 0.007$) in tau transgenic mice brains compared with their wild-type littermates or APP/PS1 mice. The preclinical examination of THK523 has demonstrated its high affinity and selectivity for tau pathology both *in vitro* and *in vivo*, indicating that ^{18}F-THK523 fulfils ligand criteria for human imaging trials.

Keywords: tau; imaging; Alzheimer's disease; dementia; PET
Abbreviations: PiB = Pittsburgh Compound-B

Introduction

The clinical diagnosis of neurodegenerative diseases such as Alzheimer's disease is typically based on progressive cognitive impairments while excluding other diseases. However, clinical diagnosis is often challenging, with patients presenting with mild and non-specific symptoms attributable to diverse and overlapping pathologies that present as similar phenotypes (van der Zee *et al.*,

Received September 23, 2010. Revised December 21, 2010. Accepted January 10, 2011

2008). Consequently, definitive diagnosis of neurodegenerative diseases is still reliant on post-mortem examination.

Post-mortem examination of the Alzheimer's disease brain is characterized by gross cortical atrophy (Wenk, 2003). Microscopically, Alzheimer's disease is characterized by the presence of extracellular β-amyloid plaques and intracellular neurofibrillary tangles (Wisniewski *et al.*, 1989; Ho *et al.*, 1994). There has been much progress in developing PET imaging radiotracers for the non-invasive detection of β-amyloid deposition (Shoghi-Jadid *et al.*, 2002; Klunk *et al.*, 2005; Rowe *et al.*, 2007, 2008; Choi *et al.*, 2009). Recent reports indicate that the best characterized and successful imaging agent Pittsburgh Compound-B (PiB), preferentially binds to fibrillar β-amyloid contained within cored and compact plaques (Klunk *et al.*, 2004; Maeda *et al.*, 2007; Ikonomovic *et al.*, 2008) and with much lower affinity to the oligomeric forms of β-amyloid (Maezawa *et al.*, 2008) that are thought to be the toxic species of β-amyloid in Alzheimer's disease (Lambert *et al.*, 2001; Walsh *et al.*, 2002; Ferreira *et al.*, 2007; Cairns *et al.*, 2009).

While amyloid imaging PET studies confirmed that β-amyloid deposition occurs well before the onset of symptoms (supporting the hypothesis that this represents preclinical Alzheimer's disease), these studies also showed the lack of correlation between β-amyloid plaque deposition and cognitive impairment in Alzheimer's disease; suggesting that markers for different and downstream effects of β-amyloid may be better suited to assess disease progression (Jack *et al.*, 2010). Therefore, new ligands are needed to explore alternative biomarkers as specific indicators of neurodegeneration. Such agents may prove invaluable in the diagnosis, follow-up and therapeutic monitoring of Alzheimer's disease and other dementias.

An obvious biomarker is tau and in particular, abnormal deposits of hyperphosphorylated tau as neurofibrillary tangles, neuropil threads and as dystrophic neurites surrounding β-amyloid plaques (a pathological hallmark of Alzheimer's disease); however, tau deposits are also characteristic of a larger group of neurodegenerative diseases termed tauopathies [i.e. sporadic corticobasal degeneration, progressive supranuclear palsy, Picks disease, as well as frontotemporal dementia and parkinsonism linked to chromosome 17 (FTDP-17)] (Lee *et al.*, 2001). Unlike β-amyloid plaque deposition, human post-mortem studies indicate that neurofibrillary tangle density correlates with neurodegeneration and cognitive impairment (Duyckaerts *et al.*, 1987, 1990; Delaere *et al.*, 1989; Arriagada *et al.*, 1992; Dickson, 1997; McLean *et al.*, 1999). Futhermore, abundant neurofibrillary tangles are not observed in cognitively unimpaired individuals, in contrast to β-amyloid plaques that are present in some non-demented people (Katzman *et al.*, 1988; Delaere *et al.*, 1990; Rowe *et al.*, 2007, 2008). Moreover, CSF-tau and phospho-tau (ptau181) have been proven useful biomarkers in the diagnosis of Alzheimer's disease (Blennow and Hampel, 2003; Ganzer *et al.*, 2003; Hampel *et al.*, 2009*a*, *b*).

Despite the quantitative assessment of CSF levels of tau and phospho-tau being reliable biomarkers of neurodegeneration (Jack *et al.*, 2010), lumbar puncture is an invasive procedure for the widespread screening of the at-risk population. Additionally, CSF measures do not provide information on regional brain tau deposition that may have clear correlates with cognition (i.e. hippocampus) and therefore, might not be able to provide important information on the therapeutic outcomes or response to current drugs aimed at modulating tau/neurofibrillary tangles (Gozes *et al.*, 2009; Hampel *et al.*, 2009*a*, *b*; Wischik and Staff, 2009).

Molecular neuroimaging with tau-specific radiotracers may provide highly accurate, reliable and reproducible quantitative statements of global and regional brain tau burden, essential for the evaluation of disease progression, therapeutic trial recruitment and the evaluation of tau-specific therapeutics (for both Alzheimer's and non-Alzheimer's disease taupathies); where tau plays a central role. Certainly, the viability of imaging disease-specific traits has been demonstrated in recent years by PET ligands such as ^{11}C-PiB (Klunk *et al.*, 2004) and ^{18}F-FDDNP, used for imaging β-amyloid deposition. Unlike PiB, it has been suggested that FDDNP also binds to neurofibrillary tangles (Agdeppa *et al.*, 2001), which may contribute to ^{18}F-FDDNP retention in the mesial temporal cortex where β-amyloid-specific tracers such as ^{11}C-PiB scarcely bind (Kepe *et al.*, 2006; Ng *et al.*, 2007; Pike *et al.*, 2007; Rowe *et al.*, 2007).

Okamura and colleagues (2005) screened over 2000 small molecules to develop novel radiotracers with high affinity and selectivity for tau pathology/neurofibrillary tangles. Consequently, they identified a series of novel quinoline and benzimidazole derivatives that bind neurofibrillary tangles and, to a lesser extent, β-amyloid plaques. Serial analysis of those compounds led to the design and synthesis of a novel imaging agent, ^{18}F-THK523. The purpose of this study was to utilize a series of *in vitro*, *ex vivo* and *in vivo* techniques to determine whether ^{18}F-THK523 satisfied a number of radioligand criteria, assessing its suitability for the quantitative imaging of tau pathology in the human brain.

Materials and methods

Materials

All reagents were purchased from Sigma, unless otherwise stated. Human β-amyloid$_{1-42}$ was purchased from the W. M. Keck Laboratory (Yale University).

Mice

Mice were housed in conditions of controlled temperature (22 ± 2°C) and lighting (14:10 h light–dark cycle) with free access to food and water. *r*Tg(TauP301L)4510 and their wild-type (CamKII) littermates were a kind gift from Jada Lewis (Dept Neuroscience, Mayo Clinic, Florida, USA) and APP/PS1 [B6C3-Tg(APPswe, PSEN1dE9)85Dbo/J] and wild-type littermates were purchased from JAX® Mice and Services. MicroPET studies employed 6-month-old rTg(TauP301L)4510 mice and 12-month-old APP/PS1 [B6C3-Tg(APPswe, PSEN1dE9)85Dbo/J] mice and their respective wild-type littermates.

Tissue collection and characterization

Human brain tissue was collected at autopsy. The sourcing and preparation of the human brain tissue was conducted by the Victorian Brain Bank Network. Alzheimer's disease pathological diagnosis was made according to standard NIA-Reagan Institute criteria (1997).

Determination of age-matched control cases were subject to the above criteria. Three Alzheimer's disease and three healthy, age-matched control cases were examined in this study.

^{18}F-labelling of THK523

Unlabelled THK523 and 2-(4-aminophenyl)-6-(2-tosyloxyethoxy)quinoline (BF241; the precursor for ^{18}F-THK523) were custom synthesized by Tanabe R&D Service Co. and confirmed for purity by reverse phase high-performance liquid chromatography, 1D nuclear magnetic resonance and mass spectrometry. ^{18}F-THK523 (Fig. 1) was synthesized by nucleophilic substitution of the tosylate precursor (BF-241). Following a 10-min reaction at 110°C, the crude reaction was partially purified on an activated Sep-Pak tC18 cartridge before undergoing semi-preparative reverse phase high-pressure liquid chromatography purification. Standard tC18 Sep-Pak reformulation produced ^{18}F-THK523 in >95% radiochemical purity. The radiochemical yield was 24% (non-decay corrected) and at end of synthesis, the average specific activity was 100 GBq/μmol (2.7Ci/μmol).

Measurement of octanol/water partition coefficient

^{18}F-THK523 (37 MBq) was added to a mixture of 3 ml 1-octanol and 3 ml of 1 M potassium phosphate buffer (pH 7.4). The mixture was shaken for 30 min, followed by centrifugation for 3 min. Aliquots (0.5 ml) were carefully taken from each phase for assay. The partition coefficient was calculated as follows: (count per minute/0.5 ml l-octanol)/(count per minute/0.5 ml buffer). Measurements were done in triplicate.

Generation and protein purification of K18Δ280K-tau

K18Δ280K-tau is a fragment of the full length protein, htau40 (Barghorn *et al.*, 2004; von Bergen *et al.*, 2006) comprising the four repeat regions of tau including residues 243–372. Polymerase chain reaction was implemented to generate K18Δ 280K-tau from plasmids kindly provided by the Mayo Clinic. Δ280K refers to the deletion of the lysine residue at position 280. DNA encoding this region was cloned into expression vector pET15b at the NcoI and XhoI sites and transfected into BL21DE3 *Escherichia coli*. Ampicillin selected *E. coli* were lysed in buffer comprising 50 mM PIPES pH 6.9, 1 mM EDTA, 5 mM dithiothreitol and protease inhibitor cocktail (Roche), sonicated on ice (6 × 30 min, with 30 s rest intervals) and the lysate was then spun at 18 000*g* at 4°C for 15 min. The supernatant was removed and added to a solution of NaCl at a final concentration of 0.5 M. The sample was then boiled for 20 min prior to centrifugation using the abovementioned conditions. The supernatant was then applied to a PD10 column (Amersham) and equilibrated in equilibration buffer (50 mM Tris pH 8.2, 20 mM NaCl, 1 mM EDTA, 5 mM dithiothreitol) and filtered prior addition to a SP sepharose column. Protein fractions were then analysed by Coomassie staining and western blot and appropriate fractions containing a single tau band were pooled, buffer exchanged into water (PD10), lyophilized and stored at −80°C.

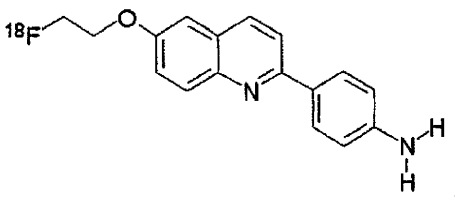

Figure 1 Chemical structure of ^{18}F-THK523 [2-(4-aminophenyl)-6-(2-fluoroethoxy)quinoline)].

Preparation of β-amyloid$_{1–42}$ and tau fibrils

Synthetic β-amyloid$_{1–42}$ was dissolved in 1× phosphate buffered saline pH 7.7 to a final concentration of 200 μM. K18Δ280K-tau was dissolved in 1× phosphate buffered saline pH 7.4 buffer to a final concentration of 20 μM. The solutions were then incubated at 37°C for 2 and 3 days, respectively, with agitation at 220 and 800 rpm, respectively (Orbital mixer incubator, Ratek). β-amyloid$_{1–42}$ fibril aggregation was confirmed via thioflavin T fluorescence spectroscopy and tau aggregation was confirmed by thioflavin S fluorescence spectroscopy; both fibril preparations were examined by transmission electron microscopy.

Thioflavin S/thioflavin T fluorescence

Aggregation of β-amyloid$_{1–42}$ fibril was confirmed using thioflavin T fluorescence (LeVine, 1999). Reactions (100 μl) comprising 20 μM β-amyloid$_{1–42}$ fibrils, 10 μM thioflavin T, 50 mM phosphate buffer were analysed at 444 nm (excitation) and 450–550 nm (emission), with an integration time of 1 s. K18Δ280K-tau fibril formation was confirmed by thioflavin S fluorescence whereby reactions comprising K18Δ280K-tau fibrils, 0.005% thioflavin S in 1× phosphate buffered saline pH 7.4 were analysed at 440 nm (excitation) and 480 nm (emission), with an integration time of 1 s. Measurements were recorded using a Varian fluorescence spectrophotometer.

Transmission electron microscopy

Fibril formation of β-amyloid$_{1–42}$ and K18Δ280K-tau was further confirmed by transmission electron microscopy following staining with uranyl acetate. Carbon-coated copper electron microscopy grids were coated with K18Δ280K-tau or β-amyloid$_{1–42}$ fibrils, as described previously (Smith and Radford, 2001). Grids were viewed on a Siemens 102 transmission electron microscope, operating at a voltage of 60 kV.

In vitro ^{18}F-THK523 binding assays

Synthetic β-amyloid$_{1–42}$ or K18Δ280K-tau fibrils (200 nM) were incubated with increasing concentrations of ^{18}F-THK523 (1–500 nM). To account for non-specific binding of ^{18}F-THK523, the reactions described above were duplicated in the presence of unlabelled 1 μM THK523. The binding reactions were incubated for 1 h at room temperature in 200 μl of assay buffer [phosphate buffered saline, minus Mg^{2+} and Ca^{2+} (JRH Biosciences); 0.1% bovine serum albumin]. Separation of bound from free radioactivity was achieved by filtration under reduced pressure (MultiScreen HTS Vacuum Manifold; Multiscreen HTS 96-well filtration plates; 0.65 μm, Millipore). Filters were washed three times with 200 μl assay buffer and the radioactivity contained within the filters was counted in a γ-counter (Wallac 1480 Wizard 3"; Perkin Elmer). Binding data were analysed with curve fitting software that calculates the K_D and B_{max} using non-linear regression (GraphPad Prism Version 1.0, GraphPad Software). All experiments were conducted in triplicate.

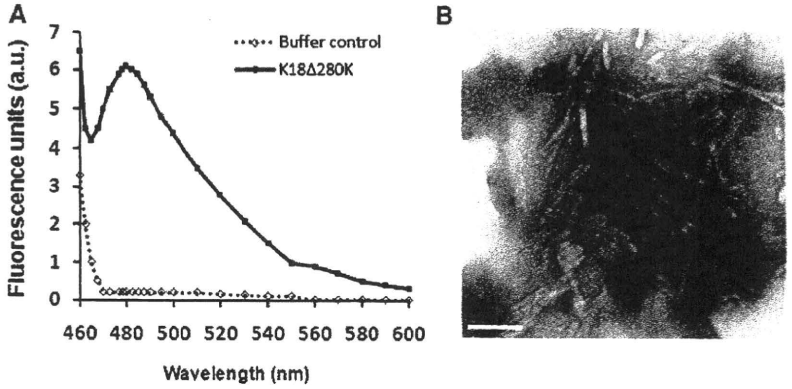

Figure 2 Characterization of K18Δ280K-tau fibrils. Recombinant K18(Δ280K)-tau was incubated with agitation (800 rpm) for 3 days at 37°C. (**A**) Graph depicting thioflavin S fluorescence, excitation/emission 440/480 nm, for K18Δ280K-tau (solid line) and no tau buffer control (dotted line). The graph for K18Δ280K-tau is indicative of positive amyloid fibril formation. (**B**) Electron microscopy image of K18Δ280K-tau fibrils. TechaniG^2 electron microscope; ×59 000 magnification. Scale bar: 50 nm. These data are representative of three independent experiments. a.u. = arbitrary units.

Immunohistochemistry and fluorescence analysis

Brain tissue from Alzheimer's disease and healthy control cases [three Alzheimer's disease (two female, one male), age range 75–83 years; three healthy controls (three female), age range 72–85 years], as well as mice (rTg4510, APP/PS1 and wild-type littermates) was fixed in 10% formalin/phosphate buffered saline and embedded in paraffin. For immunohistochemistry, 5 μm serial sections were deparaffinized and treated with 80% formic acid for 5 min and endogenous peroxidase activity was blocked with 3% hydrogen peroxide. Sections were then treated with blocking buffer (20% foetal calf serum, 50 mM Tris–HCl, 175 mM NaCl pH 7.4) before incubation with primary antibodies to β-amyloid (1E8; 1:50) or tau pAb (DAKO), for 1 h at room temperature. Serial 5 μm tissue sections were stained as follows: the first and third sections were immunostained with tau or 1E8 antibodies to identify tau tangles or β-amyloid plaques, respectively. The second serial section was stained with unlabelled THK523 to assess whether THK523 staining co-localized with the immunodetected tau tangles and/or β-amyloid plaques. Visualization of antibody reactivity was achieved with the LSAB™ kit (labelled streptavidin-biotin, DAKO) and sections were then incubated with hydrogen peroxidase-diaminobenzidine (H_2O_2-DAB) to visualize the tau tangles or β-amyloid-positive deposits. Sections were counterstained with Mayer's haematoxylin. To detect THK523 fluorescence, quenching was first performed whereby sections were first deparaffinized and tissue autofluorescence minimized by treatment of sections with 0.25% $KMnO_4$/phosphate buffered saline for 20 min prior to washing (phosphate buffered saline) and incubation with 1% potassium metabisulphite/1% oxalic acid/phosphate buffered saline for 5 min. Following autofluorescence quenching, sections were blocked in 2% bovine serum albumin/phosphate buffered saline pH 7.0 for 10 min and stained with 100 μM THK523 for 30 min. Washed (phosphate buffered saline) sections were then mounted in non-fluorescent mounting media (DAKO). Epifluorescence images were visualized on a Zeiss microscope [47CFP; filter set 47 (EM BP 436/20, BS FT 455, EM BP480/40)]. Co-localization of the THK523 and antibody signals was assessed by overlaying images from each of the stained serial tissue sections.

Autoradiography

For autoradiography, the hippocampal brain section of a patient with Alzheimer's disease (90-year-old female) was incubated with 2.2 MBq/ml of ^{18}F-THK523 at room temperature for 10 min and then washed briefly with water and 50% ethanol. After drying, the labelled section was exposed to a BAS-III imaging plate (Fuji Film) overnight. Autoradiographic images were obtained using a BAS-5000 phosphor imaging instrument (Fuji Film) with a spatial resolution of 25 × 25 μm. Neighbouring sections were immunostained using AT8 anti-tau monoclonal antibody (Innogenetics; diluted 1:20) or 6F/3D anti-Aβ antibody (DAKO; diluted 1:50).

Ex vivo biodistribution of ^{18}F-THK523

^{18}F-THK523 (0.68–1.32 MBq) was administered into the tail vein of ICR mice ($n = 20$, male, average weight 28–32 g). The mice were then sacrificed by decapitation at 2, 10, 30, 60 and 120 min post injection. The brain, blood and other organs were removed and weighed, and the radioactivity was counted with an automatic γ-counter. The percentage injected dose per gram (%ID/g) was calculated by comparison of tissue count to tissue weight. Each %ID/g value is an average ± SD of four separate experiments.

Small animal positron emission tomography imaging

All PET scans were conducted using a Philips MOSAIC small animal PET scanner with a transaxial spatial resolution of 2.7 mm full-width at half-maximum. Mice [$n = 8$ rTg4510 (four females, four males), $n = 7$ wild-type (four females, three males) mice and $n = 3$ APP/PS1 (all females) and three of their wild-type littermates (all females)] were intravenously injected with 100 μl of radiotracer comprising 3.7 MBq (0.35 μg/kg) of ^{18}F-THK523 via the tail vein. Mice were then anaesthetized using an isoflurane vaporizer with oxygen flow metre set to 5 l/min/5% isoflurane. Anaesthesia was maintained in a Veterinaire MINERVE anaesthetic assembly with the oxygen flow metre set to 2 l/min and vaporizer setting at 2%. A series of 6 × 5-min dynamic

emission scans were acquired starting at 5 min after injection. All images were reconstructed using a 3D row action maximum likelihood algorithm (RAMLA). Summed 25–35 min post-injection images were used for comparison between transgenic and wild-type mice. Image analysis was conducted using Wasabi v.2.0 software.

Statistical analysis

Normality of distribution was tested using the Shapiro–Wilk test and visual inspection of variable histograms. Statistical evaluations to assess differences in ^{18}F-THK523 binding were performed with analysis of variance (ANOVA) and a Tukey–Kramer Honestly Significant Difference test to establish differences between group means. Data are presented as mean ± SD unless otherwise stated.

Results

^{18}F-THK523 exhibits high affinity and selectivity for recombinant tau fibrils

To determine whether ^{18}F-THK523 satisfied the criteria of high affinity and selectivity for tau, the binding properties of ^{18}F-THK523 to tau fibrils was investigated and compared with β-amyloid$_{1–42}$ fibrils. A previously described truncated mutant of human tau, termed K18Δ280K-tau (Barghorn *et al.*, 2004; von Bergen *et al.*, 2006) that comprises the C-terminus of tau, including the four repeat regions and the FTDP-17 tau gene deletion resulting in the omission of lysine at position 280 (denoted Δ280K) was used for the studies. K18Δ280K-tau aggregates at low micromolar concentrations into paired helical filaments and straight filaments in the presence and absence of heparin (Perez *et al.*, 1996). Prior to conducting the binding assays, K18Δ280K-tau was formed into fibrillar structures (as monitored by thioflavin S fluorescence and transmission electron microscopy) by incubating 20 μM protein over 3 days at 37°C. On day 3, K18Δ280K-tau showed a thioflavin S fluorescence signal at ~480 nm (Fig. 2A), indicative of positive fibril formation. Fibril formation was confirmed by transmission electron microscopy with uranyl acetate staining (Fig. 2B). The β-amyloid$_{1–42}$ fibrils were generated as previously described (Fodero-Tavoletti *et al.*, 2007).

In vitro saturation studies were conducted using equimolar concentrations (200 nM, ~4.0×10^{-11} moles) of either K18Δ280-tau or β-amyloid$_{1–42}$ fibrils. While two classes of binding sites were identified on K18Δ280-tau fibrils (Fig. 3A) only one class of ^{18}F-THK523 binding sites was identified on β-amyloid$_{1–42}$ fibrils (Fig. 3B). Furthermore, there was a 10-fold higher affinity of ^{18}F-THK523 for the first class of K18Δ280-tau binding sites compared with β-amyloid$_{1–42}$ fibrils (Table 1). Overall, there was a ~5-fold higher number of ^{18}F-THK523 binding sites (B_{max}) on K18Δ280-tau fibrils, compared with β-amyloid$_{1–42}$ fibrils (Table 1).

THK523 demonstrates selectivity for tau pathology in sections of human hippocampal tissue

As a qualitative measure of its selectivity for tau pathology, THK523 recognition of tau pathology was assessed by histofluorescence and autoradiography. ^{19}F-THK523 and ^{18}F-THK523 share the same chemical structure, although ^{19}F is substituted for ^{18}F in the radiolabelled compound. For histofluorescence, unlabelled

Table 1 Binding parameters of ^{18}F-THK523 binding to fibrils

	K_{D1}	B_{max1}	K_{D2}	B_{max2}
K18Δ280K-tau fibrils	1.67	2.20	21.74	4.46
β-amyloid$_{1–42}$ fibrils	20.7	1.25		

K_D are in nM and B_{max} are in pmol ^{18}F-THK523/nmol fibrils.

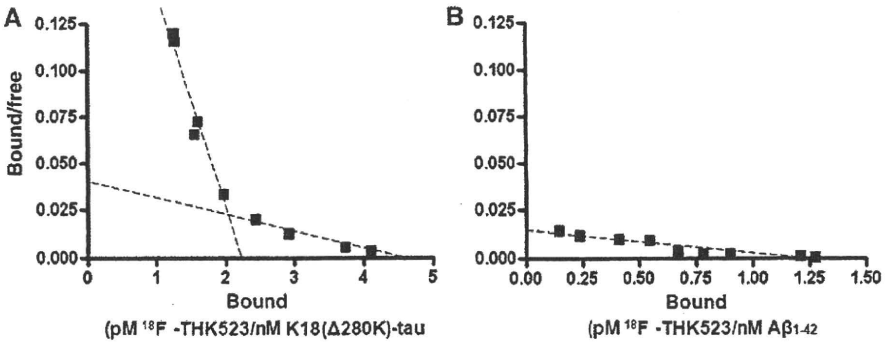

Figure 3 *In vitro* binding studies indicate two classes of ^{18}F-THK523-binding sites on K18Δ 280K-tau fibrils. Scatchard plots of ^{18}F-THK523 binding to synthetic K18Δ280K-tau (**A**) or (**B**) β-amyloid$_{1–42}$ fibrils. (**A**) Scatchard analysis identified two classes of THK523 binding sites on K18Δ280K-tau fibrils (K_{D1} and B_{max1} of 1.67 nM and 2.20 pmol THK523/nmol K18Δ280 K-tau, respectively; K_{D2} and B_{max2} of 21.7 nM and 4.46 pmol THK523/nmol K18Δ280 K-tau, respectively). (**B**) Scatchard analysis identified one class of THK523 binding sites on β-amyloid$_{1–42}$ with K_D and B_{max} of 20.7 nM and 1.25 pmol THK523/nmol β-amyloid$_{1–42}$. Binding data were analysed using GraphPad Software (Version 1.0). These data are the mean of three experiments for K18Δ280 K-tau and four experiments for β-amyloid fibrils.

THK523 binding to fixed serial sections from the hippocampus of subjects with Alzheimer's disease and age-matched controls was assessed. Contiguous sections were immunostained for β-amyloid and tau pathology with anti-β-amyloid and anti-tau antibodies, respectively. In all tissue sections examined, positive THK523 staining co-localized with tau pathology as detected in the contiguous tau immunostained section assessed (Fig. 4). THK523 failed to bind to diffuse β-amyloid plaques as indicated by the lack of co-localization with immunodetected β-amyloid pathology (Fig. 4). Likewise, autoradiography analysis in Alzheimer's disease hippocampal sections demonstrated that ^{18}F-THK523 bound to tau pathology with no ^{18}F-THK523 co-localization with immunodetected β-amyloid plaques (Fig. 5).

^{18}F-THK523 crosses the blood–brain barrier in mice

As well as being of low molecular weight (282.31 g/mol) and amenable to labelling with ^{18}F at high specific radioactivity [100 GBq/μmol (2.7 Ci/μmol)], a tau radiotracer should be adequately lipophilic to be able to cross the blood–brain barrier. The octanol/water coefficient ($logP_{oct}$) of ^{18}F-THK523 as a measure of lipophilicity, was calculated to be 2.91 ± 0.13. *Ex vivo* biodistribution studies of ^{18}F-THK523 in ICR mice, measured at 2, 10, 30, 60 and 120 min post injection, showed brain peak uptake of 2.75 ± 0.25% ID/g at 2 min post-intravenous injection (Fig. 6), indicating that ^{18}F-THK523 has adequate lipophilicity to cross the blood–brain barrier.

In vivo retention of ^{18}F-THK523 is significantly higher in tau transgenic mice brain compared with control and APP/PS1 mice

To further characterize ^{18}F-THK523 as a tau imaging radiotracer, *in vivo* microPET studies were performed to compare the retention of ^{18}F-THK523 in tau transgenic mice (rTg4510), versus their wild-type littermates (CamKII). Four independent studies were undertaken with 15 mice ($n = 8$ rTg4510 and $n = 7$ CamKII).

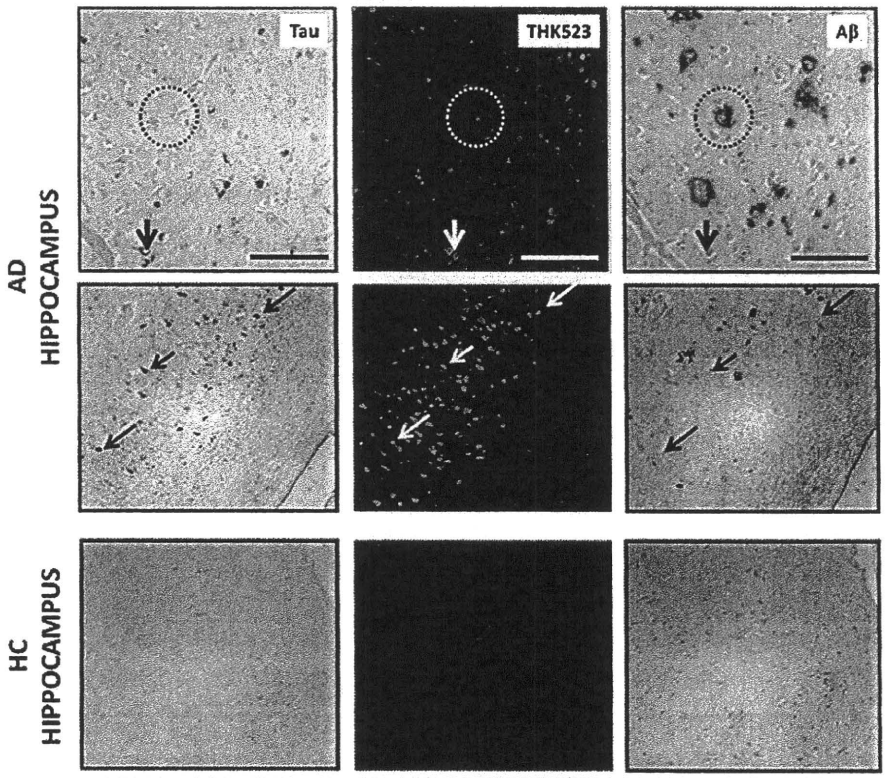

Figure 4 Histofluorescence analysis indicates that THK523 binds specifically to tau tangles with no detectable binding to β-amyloid plaques. Microscopy images of three serial sections (5 μm) from the hippocampus of a patient with Alzheimer's disease (AD) (*top* and *middle*) and a healthy control (HC) (*bottom*), immunostained with antibodies against tau (DAKO) and β-amyloid (1E8), to identify tau tangles and β-amyloid (Aβ) plaques, respectively; or stained with 100 μM THK523. Arrows indicate the location of tau tangles, while circles indicate the location of β-amyloid plaques. Positive THK523 staining appears to co-localize with tau immunostaining of neurofibrillary tangles in the hippocampus sections examined, but not to plaques. Tissue sections were imaged using a Zeiss microscope and Axiocam digital camera. Scale bars: 100 μm (*top*) and 200 μm (*middle* and *bottom*). These figures are representative of three subjects with Alzheimer's disease (two females, one male, age range 75–83 years) and three healthy controls (all female, age range 72–85 years).

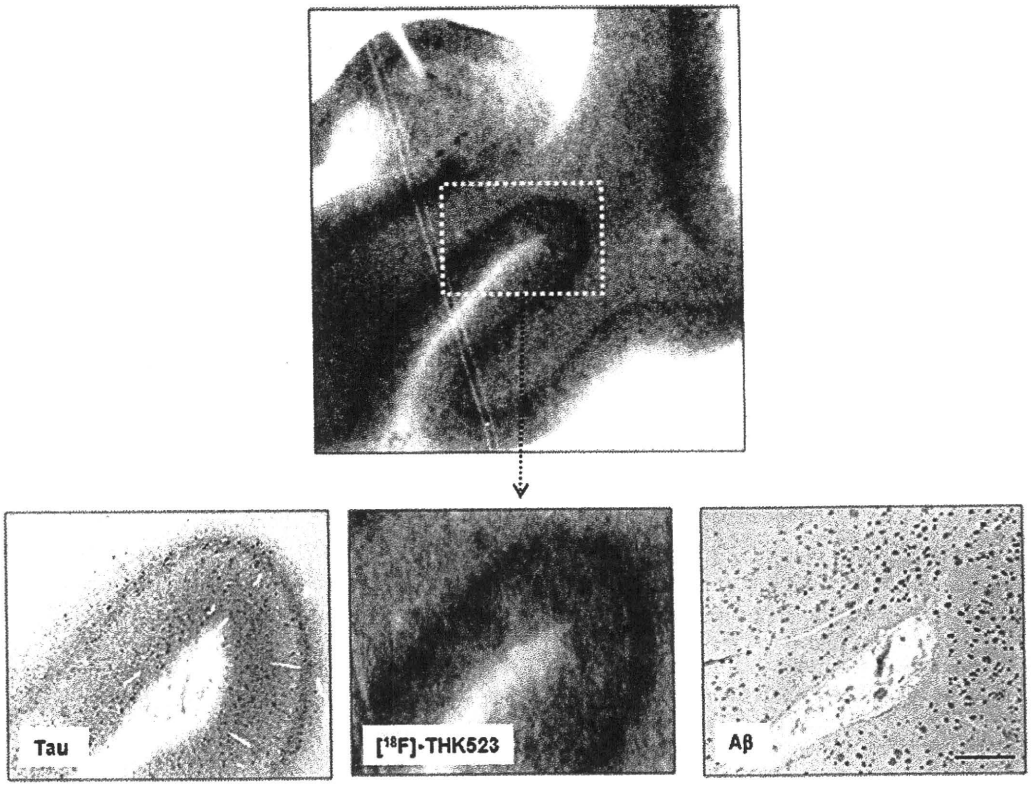

Figure 5 Autoradiography analysis indicates that ^{18}F-THK523 binds specifically to tau tangles with no detectable binding to β-amyloid plaques. (*Top*) ^{18}F-THK523 autoradiogram of Alzheimer's disease hippocampus (90-year-old female) serial section (low magnification). *Bottom*: microscopy images and autoradiogram (higher magnification) images of three serial sections (5 μm) from the hippocampus of the same Alzheimer's disease brain, immunostained with antibodies to tau (AT8, Innogenetics) and β-amyloid (6F/3D, DAKO), to identify tau tangles and β-amyloid (Aβ) plaques, respectively; or labelled with 2.2 MBq/ml ^{18}F-THK523. Positive ^{18}FTHK523 labelling appears to co-localize with tau immunostaining of neurofibrillary tangles in the hippocampus sections examined, but not to plaques. Scale bars: 500 μm. Autoradiographic images were obtained using a BAS-5000 phosphor imaging instrument (Fuji Film).

Representative microPET images are depicted in Fig. 7A and ^{18}F-THK523 time activity curves are depicted in Fig. 7C. Brain retention at ~30 min post injection of ^{18}F-THK523 was significantly higher (48%; $P < 0.007$) in the rTg4510 mice compared with their wild-type littermates (Fig. 7B). Analysis of bone, liver and intestine showed no significant differences in ^{18}F-THK523 retention (Fig. 7B), indicating a specific difference in brain uptake. Following microPET scanning, each mouse was euthanized and brains were harvested for biochemical and histofluorescence analysis. All rTg4510 mice brains examined were positive for tau overexpression as determined by western blot and immunohistochemical analysis (data not shown). Histofluorescence analysis of the same rTg4510 mice assessed by microPET identified positive THK523 staining that co-localized with immunopositive tau deposits (Fig. 8).

To further characterize the *in vivo* selectivity of ^{18}F-THK523 for tau pathology, microPET studies were conducted using the same experimental procedure in APP/PS1 transgenic mice ($n = 3$), exhibiting cerebral β-amyloid pathology but no tau deposits (Holcomb *et al.*, 1999). MicroPET analysis demonstrated that there was significantly lower retention of ^{18}F-THK523 in the brains of APP/PS1 mice, no different from the retention in their wild-type littermates ($n = 3$; Fig. 7B). Importantly, histofluorescence evaluation of rTg4510 and APP/PS1 brain tissue with 10 nM THK523 (a concentration that is achieved in the brain during PET studies), showed binding of THK523 to tau deposits in rTg4510 mice brains with negligible binding to β-amyloid plaques in the brain of APP/PS1 mice (Fig. 8).

Discussion

With the recent advances in instrumentation, image analysis and the development of new brain radiotracers, molecular neuroimaging with PET is rapidly expanding our knowledge base of neurodegenerative disease progression, improving early and accurate diagnosis, while promising to be effective in therapeutic monitoring and aiding in drug discovery and development. To date, much success has been achieved with β-amyloid radiotracers, in particular PiB being the best characterized radiotracer both *in vitro* and *in vivo*; showing selectivity for β-amyloid pathology resulting in a robust difference in ^{11}C-PiB brain retention in Alzheimer's disease

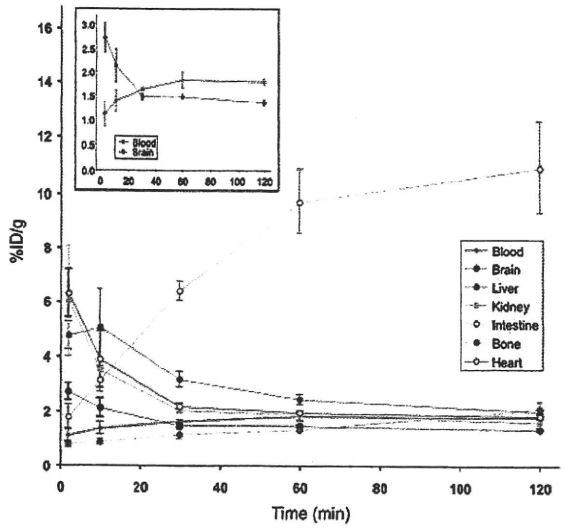

Figure 6 *Ex vivo* biodistribution studies of ^{18}F-THK523 in ICR mice. Initial uptake was highest (~6.2%ID/g) in the heart and kidney followed by a fast clearance. Liver radioactivity peaked (~5.0%ID/g) at 10 min after injection and was followed by a slow clearance, which mirrored a steady and substantial rise in radioactivity in the intestine (11%ID/g at 120 min after injection), suggesting that most of the tracer and/or its metabolites are eliminated through biliary excretion. There was a slow but steady increase in bone radioactivity, reaching a 2.1%ID/g at 120 min after injection, probably indicative of some degree of defluorination. The insert shows in better detail the brain and blood curves. Maximal ^{18}F-THK523 brain uptake (2.75%ID/g) was observed at 2 min after injection of the radiotracer, followed by a rapid clearance from the brain. Radioactivity in blood showed a different kinetic behaviour than the one observed in the brain, with a steady rise in radioactivity reaching an apparent plateau at about 60 min after injection. Uptake at each time point is expressed as percentage of injected dose per body weight (%ID/g) of ^{18}F-THK523. Curve represents the mean ± SD from four independent experiments. A total of 20 mice were examined.

compared with healthy aged-matched individuals in PET studies (Klunk *et al.*, 2004, 2005; Fodero-Tavoletti *et al.*, 2007, 2009). In addition to β-amyloid plaques, Alzheimer's disease brains are also pathologically characterized by the presence of tau pathology. Therefore, tau imaging may improve the specificity of diagnosis, allowing early detection of Alzheimer's disease and Pick's disease, where tau plays a role.

The identification and development of suitable PET radiotracer(s) is a demanding task especially given the considerable number of requirements that a radiotracer should fulfil to be deemed suitable for *in vivo* quantitative brain imaging. This study is the first to report a tau imaging radiotracer (^{18}F-THK523), that satisfies a number of criteria required for quantitative imaging of tau pathology in the human brain (Laruelle *et al.*, 2003; Nordberg, 2004; Pike, 2009). This study has shown that ^{18}F-THK523 has high affinity for recombinant tau fibrils and selectivity for tau fibrils/pathology over β-amyloid fibrils/pathology *in vitro*. Furthermore, it penetrates the blood–brain barrier, selectively highlighting tau pathology in the brains of rTg4510 tau transgenic mice *in vivo*.

In vitro saturation binding studies demonstrated that ^{18}F-THK523 binds to recombinant tau fibrils with high affinity in the low nanomole range. Typically ligands displaying affinities between 0.01–1.00 nM are deemed useful for *in vivo* quantitative PET studies. The high affinity ^{18}F-THK523-binding site (K_{D1}; 1.7 nM) exhibited >10-fold higher affinity compared with β-amyloid$_{1–42}$ fibrils (20.7 nM). Moreover, the number of high affinity ^{18}F-THK523-binding sites (K_{D1}) was almost 2-fold higher than the number of sites on β-amyloid$_{1–42}$ fibrils. In comparison to previous ^{3}H-PiB studies (Klunk *et al.*, 2005; Fodero-Tavoletti *et al.*, 2007), the affinity of ^{3}H-PiB for β-amyloid$_{1–42}$ (K_{D1}, 0.71–0.91 nM) is similar to the affinity of ^{18}F-THK523 for tau fibrils (K_{D1}, 1.7 nM). However, tau fibrils exhibit a larger number of ^{18}F-THK523 binding sites (B_{max1}, 2.20 pmol ^{18}F-THK523/nmol K18Δ280K-tau), compared with what has previously been reported for ^{3}H-PiB and β-amyloid$_{1–42}$ (1.01 pmol PiB/nmol β-amyloid$_{1–42}$) (Fodero-Tavoletti *et al.*, 2007). As the concentration of imaging radiotracers typically achieved during PET studies is in the low nanomole range, these findings strongly suggest that ^{18}F-THK523 will bind with high affinity and selectively to tau pathology under PET imaging conditions. Furthermore, as the brain area occupied by plaques is larger in comparison to neurofibrillary tangles, a >10-fold higher affinity and a larger number of ^{18}F-THK523-binding sites on tau/neurofibrillary tangles over β-amyloid plaques may prove essential in ascertaining a high tau signal over background in human PET studies (Laruelle *et al.*, 2003).

Further evidence of ^{18}F-THK523 selectivity for tau pathology was demonstrated by autoradiography and histofluorescence with positive THK523 staining, co-localizing with tau pathology and not with β-amyloid plaques in human Alzheimer's disease hippocampal sections. Importantly, even at THK523 concentrations 10 000-fold higher than those typically achieved under PET studies, THK523 failed to bind to diffuse plaques in the histofluorescence studies. There was some inconsistent staining of cored/compact plaques, suggesting that there might be some ^{18}F-THK523 binding to cored β-amyloid plaques, but only under non-PET radiotracer conditions. Similarly, variable staining of neurofibrillary tangles at high concentrations of PiB, has been reported by Ikonomovic and colleagues (2008).

In addition to high affinity and selectivity, a suitable tau radiotracer must be able to cross the blood–brain barrier to reach its target *in vivo*. The small size (molecular weight <450) (Laruelle *et al.*, 2003) and lipophilic nature of ^{18}F-THK523 [log P_{OCT} value of 2.9 ± 0.1; $-\log P_{OCT}$ values in the range of 0.9 and 3.0, show optimal entry into the brain (Dishino *et al.*, 1983)] indicates that ^{18}F-THK523 is able to penetrate the blood–brain barrier. This was confirmed in both *ex vivo* biodistribution and *in vivo* microPET imaging studies. Additionally, microPET imaging demonstrated that ^{18}F-THK523 retention was significantly higher (48%; $P = 0.007$) in the brains of rTg4510 tau transgenic mice compared with their control littermates, devoid of tau pathology; in agreement with the *in vitro* saturation and histofluorescence studies. Moreover, selectivity of THK523 for tau pathology was further supported by the ^{18}F-THK523 microPET assessment of APP/PS1 mice. These mice possess substantial cerebral β-amyloid plaque

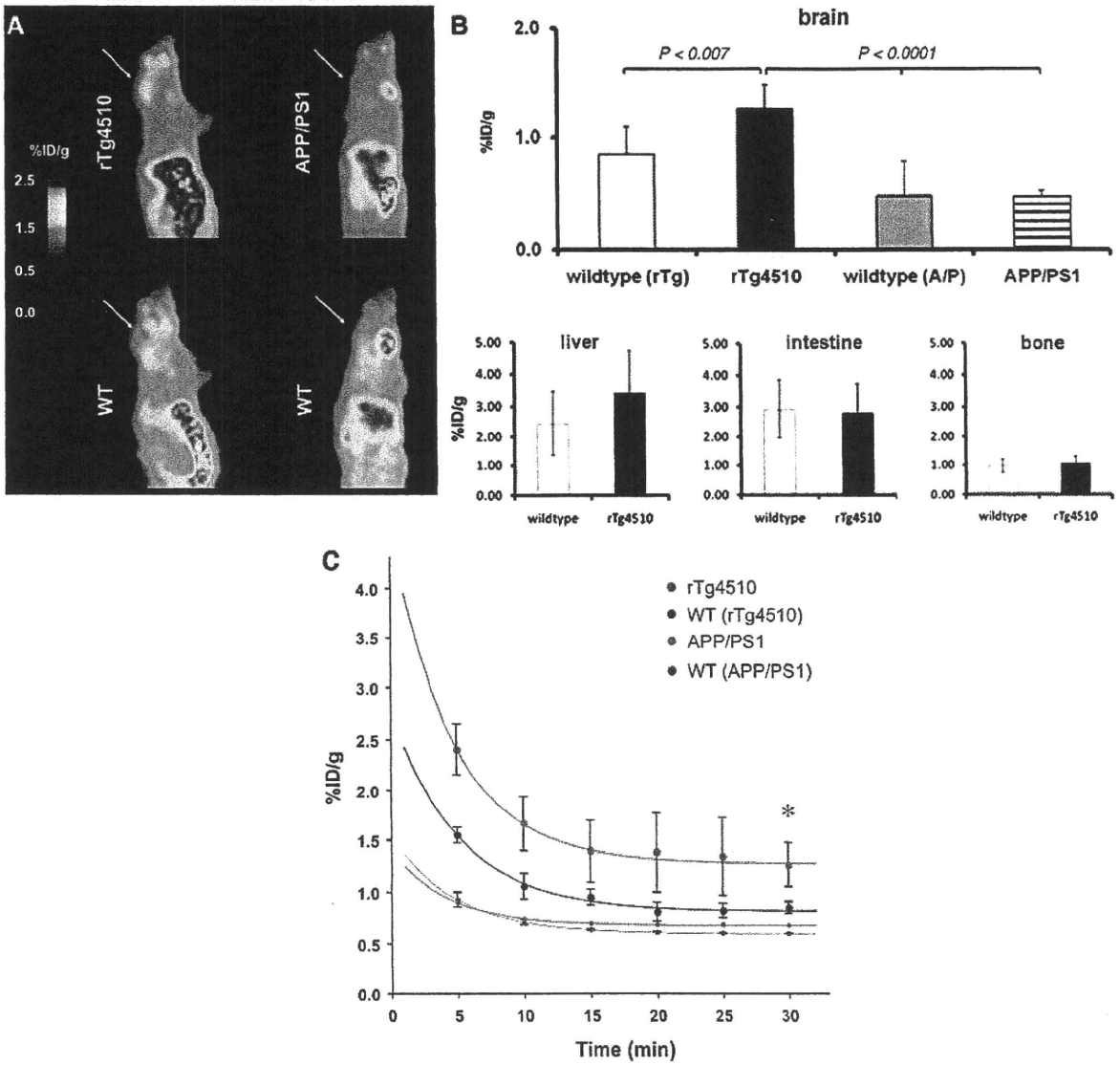

Figure 7 *In vivo* ^{18}F-THK523 microPET studies of tau and β-amyloid overexpressing transgenic mice. (**A**) Representative microPET scans at 30-min post injection of ^{18}F-THK523. rTg4510 mice (*top, left*) exhibited higher ^{18}F-THK523 brain retention compared with their wild-type (WT) littermate (*bottom, left*). Low ^{18}F-THK523 retention was observed APP/PS1 (*top, right*) versus their wild-type littermates (bottom, right). (**B**) Analysis of the ^{18}F-THK523 brain microPET data (30-min post injection) in rTg4510, APP/PS1 mice and their respective wild-type littermates revealed significantly higher (*) retention of ^{18}F-THK523 in the brain (*top*) of rTg4510 mice compared with APP/PS1 mice as well as their respective wild-type littermates. No significant differences in ^{18}F-THK523 retention were observed in the liver, intestine and bone (*bottom*). Data are presented as mean ± SD. (**C**) Brain time-activity curves of ^{18}F-THK523 microPET data expressed as percentage of injected dose per body weight (%ID/g) of ^{18}F-THK523 at each time point. Curve represents the mean ± SD of four independent studies employing $n = 8$ rTg4510 (four females, four males), $n = 7$ WT (four females, three males) mice and $n = 3$ APP/PS1 (all females) and three of the wild-type (all females) mice. Data are presented as mean ± SD.

load; however, the retention of ^{18}F-THK523 in these mice was significantly lower than in rTg4510 tau transgenic mice and not different from the retention in CamKII mice or their own wild-type littermates; suggesting that THK523 does not significantly bind to β-amyloid plaques and is selective for tau pathology *in vivo*.

Analysis of ^{18}F-THK523 biodistribution in the microPET studies showed no significant differences in ^{18}F-THK523 retention in the liver, intestine or bone between rTg4510 tau transgenic and wild-type mice. ^{18}F-THK523 retention in bone is indicative of some degree of defluorination (Van Dort *et al.*, 1995). *In vitro* stability testing showed that ^{18}F-THK523 was stable *in vitro*, suggesting that defluorination most likely occurs post-injection (data not shown). However, as the degree of free ^{18}F-bone retention is similar in both transgenic and control mice, the free ^{18}F does not

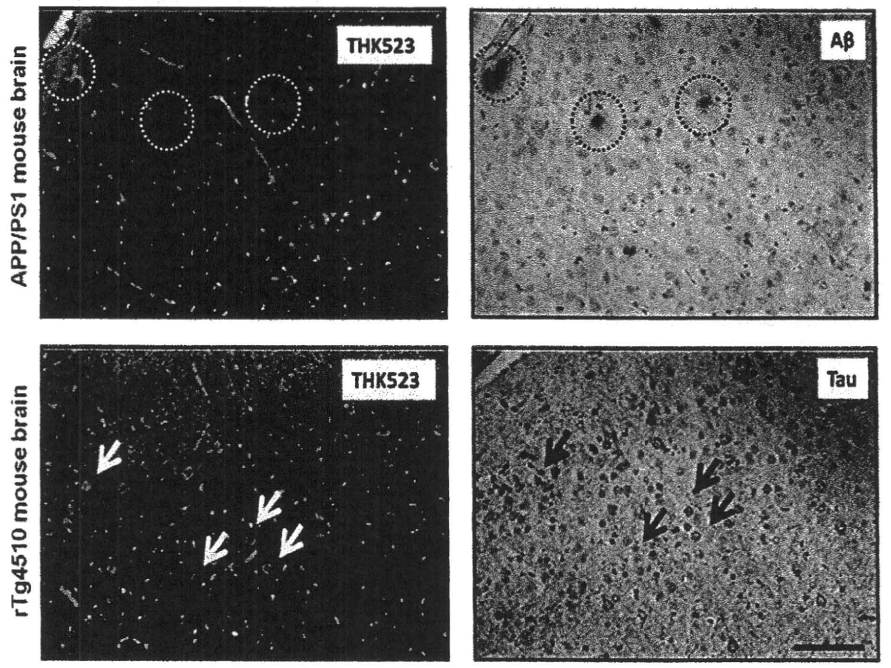

Figure 8 Co-localization of THK523 staining with tau pathology. Microscopy images of two serial sections (5 μm) from brains of rTg4510 and APP/PS1 mice immunostained with either tau (DAKO) or β-amyloid (1E8) antibodies, to identify tau tangles and β-amyloid (Aβ) plaques respectively; or stained with 10 nM THK523. Arrows indicate the location of tau tangles while circles indicate the location of β-amyloid plaques. Positive THK523 staining co-localize with tau immunostaining of neurofibrillary tangles, but not with β-amyloid plaques. Tissue sections were imaged with a Zeiss microscope and Axiocam digital camera. Scale bars: 100 μm. These data are representative of four independent studies employing eight rTg4510 and three APP/PS1 mice.

contribute differentially to the retention of ^{18}F-THK523 in the mouse brain. Similarly, as was observed in the *ex vivo* biodistribution studies, accumulation of radioactivity was observed within the intestine and liver of both rTg4510 and their control littermates indicating that most of the tracer and/or its metabolites were eliminated rapidly from the body through biliary excretion. Both tau transgenic and control littermates exhibited similar, low expression levels of tau in the liver (data not shown), further suggesting that ^{18}F-THK523 liver retention was due to the metabolic processing of ^{18}F-THK523 and not attributable to tau expression.

In conclusion, ^{18}F-THK523 is a novel tau radiotracer that fulfils the major criteria necessary for an 'ideal' PET radiotracer (Laruelle *et al.*, 2003; Nordberg, 2004). In addition to the abovementioned properties, THK523 was successfully labelled with ^{18}F with high specific activity. The relatively longer half-life of ^{18}F (110 min) precludes the need for an onsite cyclotron, allowing widespread distribution.

The clinical application of ^{18}F-THK523 as a selective tau imaging biomarker will provide important information regarding tau pathophysiology in Alzheimer's disease and non-Alzheimer's disease tauopathies, allowing correlation of brain tau load with cognitive function, monitoring disease progression and evaluation of therapeutic efficacy of newly developed drugs; especially aimed at modulating tau pathology (Gozes *et al.*, 2009; Hampel *et al.*, 2009*a*, *b*; Wischik and Staff, 2009). This study provides an important and critical step in defining the role of ^{18}F-THK523 as a tau specific PET radiotracer.

Acknowledgements

We thank Fairlie Hinton and Geoff Pavey from the Victorian Brain bank Network for sourcing and preparation of the human brain tissue.

Funding

National Health and Medical Research Council of Australia (in part); Neurosciences Victoria and the Ministry of Health, Labour and Welfare, Japan (in part); Industrial Technology Research Grant Program in 2009 from New Energy and Industrial Technology Development Organization (NEDO) of Japan(in part); AAR Viertel Fellowship (to M.T.F.-T.); NHMRC Senior Research Fellowship (to R.C. and K.J.B.). Perpetual Trustees H & L Hecht Trust.

References

Agdeppa ED, Kepe V, Liu J, Flores-Torres S, Satyamurthy N, Petric A, et al. Binding characteristics of radiofluorinated